Chemical Engineering Science 63 (2008) 5860 – 5869

Contents lists available at ScienceDirect

Chemical Engineering Science

journal homepage: www.elsevier.com/locate/ces

Experimental comparison between acoustic and pressure signals from a bubbling flow

A. Vazquez [a,*], R. Manasseh [b], R.M. Sánchez [a], G. Metcalfe [b]

[a] Universidad Autónoma Metropolitana—Iztapalapa I.R.E., Av. San Rafael Atlixco No. 186, Col. Vicentina, C.P.09340, México D.F., Mexico
[b] Fluid Dynamics Group, CSIRO Materials Science and Engineering, PO Box 56, Highett, VIC 3190, Melbourne, Australia

ARTICLE INFO

Article history:
Received 17 February 2008
Received in revised form 2 August 2008
Accepted 22 August 2008
Available online 17 September 2008

Keywords:
Bubbling
Flow rate
Flow regimes
Chaotic
Correlation dimension
Time delay

ABSTRACT

Experiments were performed on both the acoustic and pressure signals produced by bubbles formed from an underwater nozzle. The data were analyzed by a comprehensive set of spectral and nonlinear-dynamical techniques. As air flow rates increase, it is well known that such flows became chaotic. However, the present study of both acoustic and pressure signals showed that chaos could appear in different regimes and was manifested in different ways in the acoustic and pressure signals. The use of different time delays for the chaotic analysis of acoustic and pressure signals were found necessary. The acoustic signals offer data primarily on the bubble size while the pressure signals offer data primarily on the bubble production rate. The present results suggest that chaos can appear in the bubble size and bubble production rate independently.

1. Introduction

Bubbling flows have great importance in many industrial processes (Shah and Deckwer, 1985; Krishna et al., 1997; Koynov and Khinast, 2004; Raffensberger et al., 2005), in biological applications (Walter and Blanch, 1986; Prakash et al., 2001; Klein et al., 2002), and also in geophysical behavior (Johnson 1986; Loewen and Melville, 1991; Vergniolle and Brandeis 1996; Leifer and Patro, 2002; Graham et al., 2004). In bubbling flows, the bubble production rate (also called the bubbling or sparging rate) determines the kind of flow regime in the system (Clift et al., 1978). Gas bubbles (in a given ambient liquid) are typically generated by porous ceramic stones, sieve plates, capillary tubes, electrical fields, or flexible orifices, etc. In many experimental studies the flow regimes are classified with respect to bubble production frequency or air flow rate (Q). Sato et al. (1979) described three regimes of bubbling: periodic bubbling, dispersed bubble production, and sparking-larger bubble production for those bubbles generated with an electrical field. Similarly, Shin et al. (1997) outlined three bubbling modes—dripping, an erratic mixed mode, and a spray mode.

To characterize these bubbling regimes several techniques are used, such as high speed video (Teresaka et al., 2000; Lee et al., 2003; Oliveira and Ni, 2004), impedance tomography (George et al., 2000; Wang et al., 2002; Zenit et al., 2003), pressure transducers (Johnsson et al., 2000; Ruzicka et al., 2000; Barghi et al., 2004; Chilekar et al., 2005), acoustic hydrophone probes (Zukowski 2001; Manasseh et al., 2001, 2004; Vazquez et al., 2005; Al-Masry et al., 2005, 2007), and X-ray emissions (Xie and Tan, 2003; Hulmea and Kantzasa, 2004; Hubersa et al., 2005). However, pressure and acoustic transducers are widely used because of their low price, high resistance to corrosive liquids and their ability to operate at elevated operational temperatures and pressures.

Of course, both `pressure' and `acoustic' transducers measure pressure, but over very different frequency bands. Pressure transducers are designed to measure static pressure although they can also respond to fluctuations in pressure up to a few hundred Hz. Acoustic transducers are designed to measure only fluctuations in pressure, and are typically used for frequencies above a few hundred Hz.

It is important to note that two very different natural timescales of pressure fluctuations will occur in bubbling flows. As each bubble is pinched off and rises, the flow created in the liquid generates a pressure fluctuation in the liquid. Signals obtained by pressure transducers are dominated by this bubbling-rate signal, which is in the order of 10 Hz (e.g., Clift et al., 1978; Manasseh et al., 2001). However, the bubble formation also causes the gas trapped in the bubble to oscillate volumetrically, due to the compressibility of the gas. This is a much higher frequency process, given by the Minnaert frequency

$$f_0 = \frac{1}{2\pi}\sqrt{\frac{3\gamma P_\infty}{\rho}} \cdot \frac{1}{R_0}, \tag{1}$$

where (Minnaert 1933), f_0 is the frequency in Hz, P_∞ is the absolute liquid pressure, γ is the ratio of specific heats for the gas, ρ is

* Corresponding author.
E-mail address: zeta24_75@yahoo.com (A. Vazquez).

0009-2509/$ - see front matter © 2008 Elsevier Ltd. All rights reserved.
doi:10.1016/j.ces.2008.08.032

the liquid density, and R_0 is the equivalent bubble radius (the radius assuming the bubble is a spherical volume). Thus, the acoustic transducer signals are dominated by the Minnaert frequency which is in the order of 1000 Hz. Thus, it might be expected that analyses of simultaneous measurements of acoustic and pressure signals would reveal different phenomena. Owing to this difference in timescales, cross-correlation of the two signals would not be meaningful; indeed, the `acoustic' signals would be correlated with the `pressure' signals at frequencies of the order of 10 Hz, in which band both transducers are measuring exactly the same quantity: low-frequency pressure fluctuations due to the rate of bubble detachment.

The pressure fluctuations (time series) are generally analyzed by power spectral density (PSD) and Fourier spectral (FS) methods and are applied in orifice or nozzle systems or fluidized beds (Fan et al., 1981; Satija and Fan, 1985; Sun et al., 1994; Johnsson et al., 2000; van der Schaaf et al., 2002). However, in the majority of cases, these methodologies are qualitative. In recent years, nonlinear dynamical systems (or `chaotic') analysis has been introduced for bubbling-flow regime characterization, because this methodology can extract much information hidden in apparently random signals. Some researches have used auto-regressive moving average (ARMA) models for linear dynamics analysis in time series data of physical events (such as sunspots, environmental data, etc.) but these models have been unable to explain the events in a satisfactory manner (Fan and Yao, 2005).

Ruzicka et al. (2000) introduced nonlinear dynamical systems analysis to orifice bubbling signals. Mosdorf and Shoji (2003) applied nonlinear analysis (the Lyapunov exponent) in order to explain the changes in bubbling flow, and they indicate that the largest Lyapunov exponent is increased when the air volumetric flow rate changes from 500 to 1500 ml min^{-1}. Other authors (Nguyen et al., 1996; Tufaile et al., 1999; Tufaile and Sartorelli, 2000) use bifurcation plots to illustrate that the complex dynamics in the bubbling flow result from the variation in some process input variable, such as the flow rate.

Liu (2003) employed nitrogen and distilled water as the gas and liquid phase respectively, in an acrylic column with an inner diameter of 0.07 m and a height of 1.0 m. Liu observed that when the correlation dimension (D_2) for $Q = 73$ ml min^{-1} is about 2.5 (for intermediate values of the hyper-sphere radius r to be decribed in Section 3.2 below), the process can be identified as periodic bubbling; when Q is in the range of 168–250 ml min^{-1}, the D_2 values first increase, indicating the onset of chaotic bubbling, but later decrease, which may result from a self organization of the bubbling system due to bubble–bubble interactions. When Q increases further (357–998 ml min^{-1}) an abrupt increase in D_2 is observed, indicating that the bubbling process begins to undergo another re-organization. The increase and drop in D_2 shows that the bubble hydrodynamics changes from a primary chaos to a high degree of chaos, and in this range of Q, break-up and coalescence of the bubbles dominate the bubbling process.

Zhang and Shoji (2001) observed four regimes for an air volume flow rate range of 100–2000 ml min^{-1}, in which regimes of single bubbling, pairing, double, and triple coalescence are found. For Zhang and Shoji (2001), the pairing-bubble regime was the most interesting from the point of investigation from chaos theory, and therefore, their nonlinear analysis was done for a range of 435–1500 ml min^{-1}.

Cieslinski and Mosdorf (2005) used a hydrophone to measure acoustic signals of air bubbling from a submerged 0.9 mm glass nozzle. Based on data from a laser interrupted by the bubble formation as well as hydrophone data, they obtained the maps of chaotic attractors for several volume flow rates (42, 125, and 233 ml min^{-1}). All attractors displayed a chaotic character. They did not measure pressure signals as well.

Although the previous methodologies (PSD, FS, chaotic) have been applied to pressure signals, apart from Cieslinski and Mosdorf (2005) the literature lacks nonlinear dynamical systems (chaotic) studies on acoustic signals in bubbly flow. The present work applies chaotic analyses to acoustic as well as pressure signals measured simultaneously in the same system.

In the present work, we obtained the time series data of the multi-spectral pressure and acoustic signals for air bubbles generated in distilled water, for Q in the range of 70–305 ml min^{-1}. The correlation dimension D_2 is calculated for these pressure–acoustic fluctuations and three bubbling flow regimes are observed.

2. Experimental set-up

The experimental sketch is shown in Fig. 1. The air is provided by a compressor (Cole-Parmer, Quiet Vacuum, USA) at a pressure

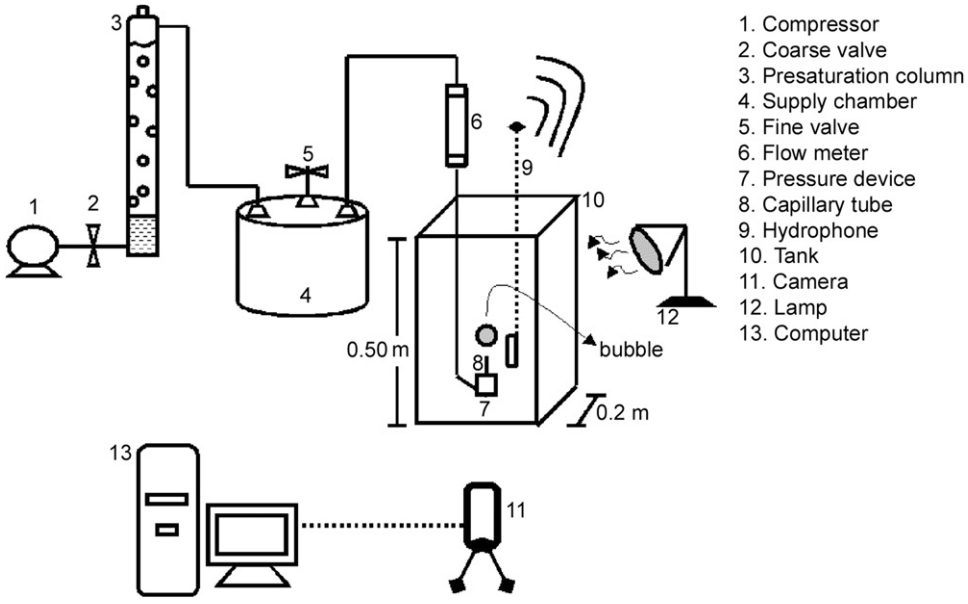

Fig. 1. Experimental set-up in which both acoustic (wireless hydrophone) and pressure signals (differential sensor) channels are sampled simultaneously over 60 s giving 2.6×10^6 data points per channel.

of 34.5 kPa. Air is pumped into a pre-saturation column which prevents rapid changes in bubble volume after its pinch-off, owing to inflow to the bubble of water vapor (Manley, 1960), and is controlled by a coarse valve. The air then passes through a cylindrical supply chamber (3.7×10^{-3} m^3) which maintains a constant pressure that could be varied between 0 and 4.4 kPa. Subsequently, the air flow is controlled and measured by a fine valve and a flow meter (NO.11/1–350 ml min^{-1}, and Gilmont Inc., St. Louis MO. USA), respectively. The air bubbles are generated using a glass capillary tube (Drummond Scientific, Broomall PA, USA), with an inner diameter of 990 ± 10 μm inserted in an acrylic base centered in the glass tank of 0.2×0.2×0.5 m. The tank dimensions ensured wall effects during bubble formation, pinch-off, and acceleration within the tank were negligible (Filderis and Whitmore, 1961). The tank was filled to a height of 0.4 m with distilled water (Thermal-Line, USA) and maintained at $22 \pm 0.5\,^{\circ}$C. The vertically oriented capillary tip was at a depth of 0.09 m.

The air-pressure fluctuations are measured with a differential pressure device (Motorola MPXV5004G series, Denver, Colorado, USA) installed in the capillary base, and the passive acoustic signals are obtained by a piezoelectric wireless hydrophone built in the laboratory (Vazquez et al., 2005) and located an optimal 5 cm away from the bubble generator in order to minimize any perturbation to the bubble dynamics and to maximize the quality of the acoustic signal as much as possible (Manasseh et al., 2001). The tank was designed to be large enough to neglect reverberation (Kinsler and Frey 1962; Nikolovska, 2005; Manasseh et al., 2008). Both pressure and acoustic time series are recorded simultaneously with an audio card (Sound Blaster 64 PCI) at 44.1 kHz/16 bit using the external and microphone inputs for the pressure and acoustic perturbations, respectively. The data acquisition time was 60 s giving a total of 2.6 million data points recorded for each Q value. The bubbling flow regimes are captured by a high speed camera (MotionScope 8000S, Lake Image Systems, NY, USA) at a frame rate of 1000 frames s^{-1} and a resolution of 160×140 pixels on an 8-bit gray scale; the images are stored in the PC. Illumination is provided by 500 W halogen lamp shining on the back wall of the tank and a diffusion screen decreases small-scale inhomogeneity in the illumination.

3. FS and chaotic time series analysis

3.1. Fourier spectral (FS)

The FS method is frequently used to characterize flow regimes and for verification of the relationships for scale-up, simulations and physical phenomena in fluidized beds (Van der Schaaf et al., 1999, 2002; Chilekar et al., 2005). The previous studies concentrated on the dominant frequency as the main characteristic of the flow. In addition, with this tool a preliminary identification of dynamic changes of the bubbling flow regimes is possible, and perhaps, other analysis tools are needed to further identify and explain the complex behavior.

In this work the FS was realized by Adobe Audition v1.0 package using a Welch (Gaussian) window with an FFT size of 65536 points.

3.2. Correlation dimension (D_2)

The correlation dimension is one measure of the fractal dimension of a chaotic system; others are the box-counting, similarity or Lyapunov dimension of a chaotic system. The correlation dimension is one of the most important measurements of the chaotic behavior, because it quantifies the complexity of the chaotic attractor as well as providing a link to self-similar property of the fractal sets. The correlation dimension is related to the number of ordinary differential equations required to describe the system. Previous authors (Johnsson et al., 2000; Lin et al., 2001; Liu, 2003; Mosdorf and Shoji, 2003) have utilized D_2 for bubbling regime characterization in bubble columns, and fluidized beds. In our case, D_2 is given by

$$C(r) \approx r^{D_2}, \tag{2}$$

where

$$C(r) = \frac{1}{N}\sum_{k=1}^{N}\frac{1}{N}\sum_{n=1}^{N}\theta(r - |\vec{y}(n) - \vec{y}(k)|), \tag{3}$$

with θ being the Heaviside step function and r the radius of a dimensional ball (a hyper-sphere), (Lin et al., 2001). From Eq. (2), D_2 is the slope of ln $C(r)$ vs. ln r. In Eq. (3), $\vec{y}$ is a vector of dimension d, computed from the original time series data.

In this type of analysis the time delay (τ) and the embedding dimension (d) are very important parameters for extraction of the correlation dimension. With proper selection of the time delay and the embedding dimension, the chaotic attractor is revealed. For this reason, choice of the time delay is crucial at the very beginning of the reconstruction process. The time delay cannot be too small (or the axes of the d dimensions would be too closely related) and cannot be too large (or information would be lost between axes). Similarly, if d were selected too small, the delayed phase space cannot completely unfold the attractor and false nearest neighbors would occur. As d is increased above the correct (or saturation) value of the correlation dimension, D_2 will cease to increase, since adding more embedding dimensions will not reveal more dimensions of the attractor. In a simple analogy, embedding a one-dimensional object (a line) in a two-dimensional space (a plane) confirms that it has a dimension of one, but embedding it in a three-dimensional space (a volume) does not reveal anything further. As noted above, in the present work, the acoustic and pressure signals have inherent timescales that are very different. Hence, the use of different τ is likely to be necessary for the acoustic and pressure signals. In the present work the D_2 calculation was realized by visual recurrence analysis (VRA) v.4.9 software and general indications of the delay times are calculated using the average mutual information algorithm (AMI). Abarbanel (1996) states that the AMI is a kind of nonlinear autocorrelation function that can be used to determine when two measurements of the data, $s(n)$ and $s(n+\tau)$, are independent enough of each other to be useful as co-ordinates in a time delay vector, but not so independent as to have no connection with each other at all. The actual prescription suggested is to take the τ where the first minimum of the AMI occurs as the value to use in time delay reconstruction of phase space. Abarbanel (1996) notes that the choice of the first minimum of the AMI is reminiscent of the choice of the first zero of the linear autocorrelation function and that this choice is the optimum linear choice from the point of view of predictability, in a least squares sense, of $s(n+\tau)$ from knowledge of $s(n)$. However, for some phenomena Abarbanel (1996) cannot recommend this choice at all, noting that such a linear choice has no clear relation to the nonlinear process relating $s(n)$ and $s(n+\tau)$.

Thus, for the results of the present paper, a wide range of τ values were examined for each case, including but not limited to those suggested by AMI, and the ones presented below gave the most reasonable results, as determined by criteria such as saturation of the correlation dimension.

3.3. Recurrence plot (RP)

The RP can thus help determine the correct choices for both the embedding dimension and the embedding delay (Eckmann et al., 1987; Mindlin et al., 1991). Atay and Altintas (1999) indicate that the two-dimensional graph can contain intriguing patterns; however, they argue that many of these patterns are artifacts of the way the

embedding is done, and if the embedding parameters are correctly chosen, all one should see are simple horizontal segments, and if the reconstruction actually represents the true dynamics, this can be directly observed in the RP.

The RP is a device displaying how the reconstructed trajectory comes close to it self (Atay and Altintas 1999). The plot is constructed following the definition of Atay and Altintas (1999). Let δ be a fixed positive number, and define the array

$$a_{ij} = \begin{cases} 1 & \text{if } \|v_i - v_{i+j}\| < \delta \\ 0 & \text{otherwise} \end{cases}, \quad i,j = 1,2,\ldots, \tag{4}$$

where the v_k are the vectors obtained by

$$v_k = (x_k, x_{k-\tau}, \ldots, x_{k-(d-1)\tau}), \tag{5}$$

and $\|\cdots\|$ denotes the usual Euclidean norm. The quantity δ is a measure of closeness and is usually expressed as a percentage of the diameter of the attractor or the standard deviation of the time series data. The RP is obtained by plotting a point on the i–j plane whenever $a_{ij} = 1$.

Nonhorizontal lines on a RP indicate phase space vectors that are co-incidentally close but point in opposite directions, representing an incorrect choice of embedding dimension or time delay (Atay and Altintas, 1999). Hence, establishing an RP without nonhorizontal patterns is the first step in the determination of the correct embedding parameters. Although in this case Atay and Altintas only consider time series generated by smooth dynamical systems, they assume that the time interval between measurements is sufficiently small to capture the smoothness of the trajectories.

Kung-Sik and Howell (2001) show RPs for discrete time data in which diagonal lines are observed, and if these lines do not include isolated points, they state that the embedding dimension is determined correctly.

4. Results and discussion

The pressure–acoustic time series are shown in Fig. 2. For $Q = 70\,\text{ml min}^{-1}$, the pressure and acoustic signals show a frequency of ≈ 25 bubbles s^{-1} (each maximum peak corresponding to a bubble departure) and the production of solitary bubbles are clearly observable (Fig. 3). For $Q = 240\,\text{ml min}^{-1}$, the pressure fluctuations indicate a frequency of ≈ 35 bubbles s^{-1}, while in the acoustic case, it is no longer possible to identify bubble detachment, and coalescence at the tip of the capillary tube is observed (Fig. 3). When $Q = 305\,\text{ml min}^{-1}$, the pressure signal indicates a frequency of ≈ 45 bubbles s^{-1}, the acoustic signals are completely superimposed and an air jet is observed at the capillary tip (Fig. 3).

Applying simple FS to the time series data we obtain Fig. 4. In the pressure case the continuous thick, continuous thin and dashed lines represent low ($70\,\text{ml min}^{-1}$), moderate ($240\,\text{ml min}^{-1}$) and high ($305\,\text{ml min}^{-1}$) air flow rates, respectively. When the air flow is increased, the bubbling-rate frequency peak is moved to the right side in the figure; this displacement is a typical observation in any sparging system (Clift et al., 1978); it was, for example, observed by Fan et al. (1986) for glass particles in a fluidized bed and Liu (2003) in a gas–liquid column. In the acoustic case, the frequency peak is

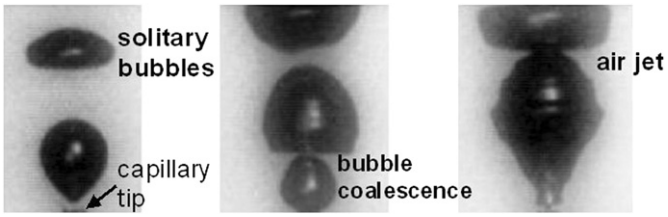

Fig. 3. Bubble generation photographs.

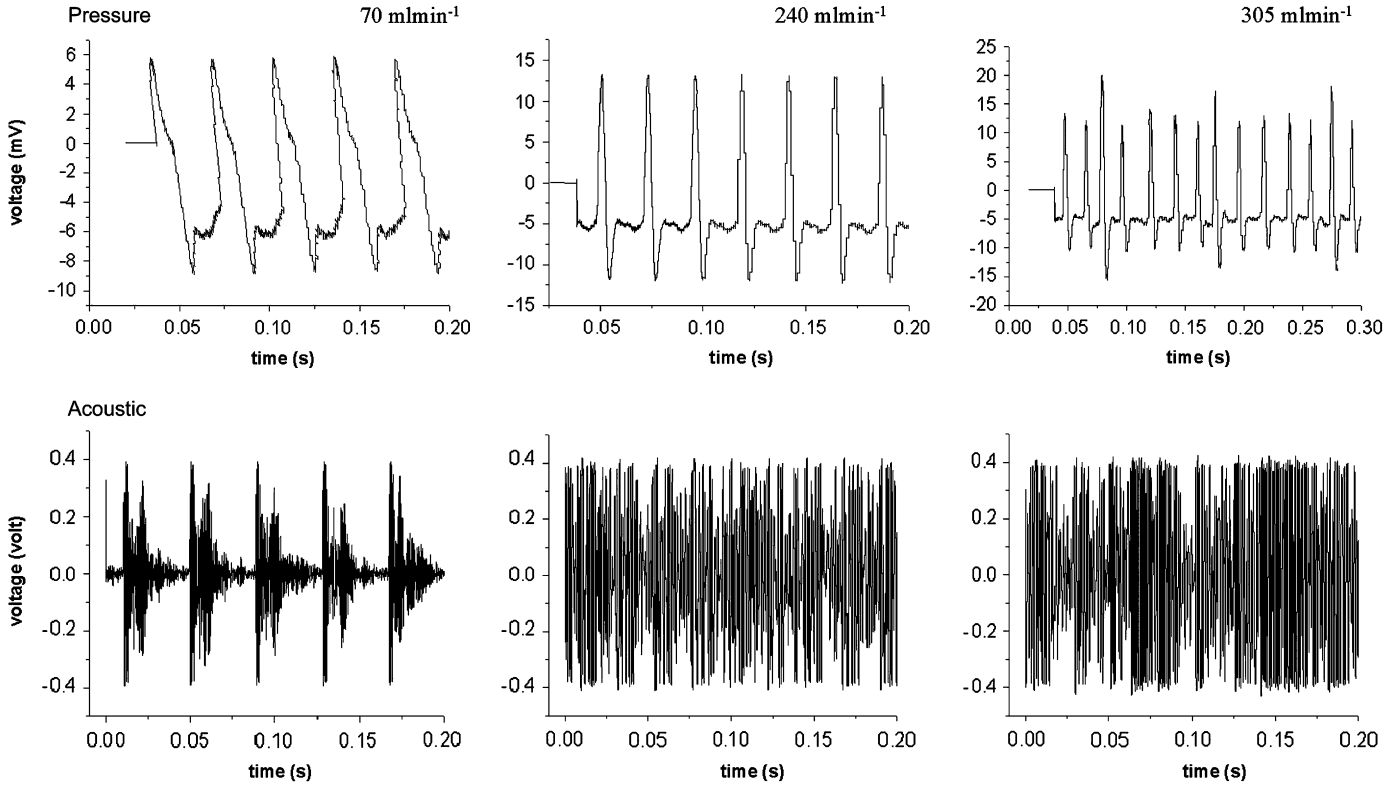

Fig. 2. Pressure and acoustic time series fluctuations for 70, 240, and $305\,\text{ml min}^{-1}$ air flow rate.

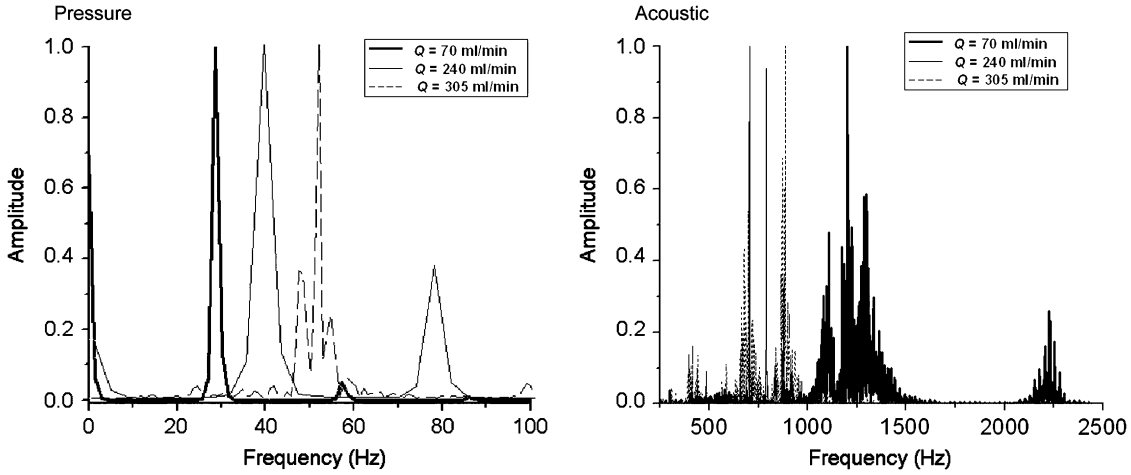

Fig. 4. Fourier spectra for pressure and acoustic data in which the amplitude is normalized, for three different flow rates, $Q = 70$, 240, and 350 ml min^{-1}; legend is on plot.

moved to the left side of the figure. This indicates that the bubble size changes from 1500 to 2285 μm and finally to 2285–4975 μm for the low to high Q values, using Minnaert's relation (Eq. (1), Minnaert, 1933) to calculate the bubble sizes.

With the FS method three bubbling regimes for each air flow rate can be distinguished, called disperse, chaotic-disperse transition and random-chaotic. But generally the FS methodology does not give clear results for most bubbly flow regimes (Briens and Ellis, 2005).

In Fig. 5 the correlation dimension plots for the pressure and acoustic signals are shown. The graphs were generated using a time delay ranging from 1 to 10. The embedding dimension (d) reaches saturation values of 6 and 16 for pressure and acoustic cases, respectively, when the air flow rate is low, while for moderate air flow rate the saturation value is reached only for the pressure case and this not is observed in the acoustic case. This implies that the time delays chosen fail to reveal the attractor for moderate flow rates only. For the high air flow rate the saturation value is 10 and 14 for the pressure and the acoustic signals, respectively.

The present saturation D_2 values ranging from approximately 5 to 20 are consistent with those reported by Lin et al. (2001) and Liu (2003). However, an interesting subtlety is revealed on examination of Fig. 5. In all cases, the embedding dimension (d) value at which D_2 saturates is significantly greater than the corresponding D_2 value. For example, in Fig. 5A, an embedding dimension d of 6 is required to reveal that the pressure signal has a saturation D_2 value of about 2. In principle, as noted in Section 3.2, d needs to be greater than the correct value of D_2 in order to reveal the correct D_2, but once d is larger than the correct D_2, no further details of the attractor should be revealed. In theory, $d >= D_2$ is sufficient (Ding et al., 1993; Nerenberg and Essex, 1990); however in the presence of noise, it may be necessary to have $d >= D_2+1$ (Takens, 1981). Checks with the software on artificial sine-wave signals confirmed this principle is obeyed by the software, and thus the results of Fig. 5 need a physical explanation. One possible reason is that both pressure and acoustical signals contain low levels of noise that makes their true fractal dimension difficult to determine, forcing the software algorithm to increase d to try to reveal further dimensions that are not present.

Although the AMI function was used to give general guidance, it must be noted that sometimes, depending on the data, the usage of another method of defining τ gives better results; examples are the degree of separation function, or Lyapunov exponents. In practice, irrespective of the method used to define τ, in the present work the analysis was repeated several times with different τ values empirically chosen around those suggested by the AMI function. The delay times used in Fig. 5 are those delay times, τ, for which it was possible to observe some saturation values for D_2. The τ values obtained using the AMI function were 4, 6, and 4, respectively, for the low, moderate, and high air flow rates of the pressure case, and 9, 10, 15, respectively, for acoustical case. With these actual values, no saturation of the correlation dimension saturation was reached. In this sense the AMI function was a tool for the estimation of approximate values for τ; however is it clear that the actual values were inappropriate. At least for the results of the present paper, this may be an inherent feature of the presence of noise in the data and possibly to the complication introduced by the two timescales.

Now, using the method of delays (MOD), the phase space is reconstructed for the three air flow rates cited above, and are shown in Fig. 6. The time delays were $\tau = 10$, 1, 9, respectively, for the three flow rates of the acoustic case and $\tau = 1$, 4, 1 for the pressure case. The acoustic case (Fig. 6A, B, C) will be discussed first. It is interesting to observe that for the acoustic case the points are close, forming a circular shape for the low flow rate (Fig. 6A), indicating that a good reconstruction has been performed in this case. Meanwhile when the air flow is increased the points are close to diagonal implying that the delay time is too small for an appropriate reconstruction (Fig. 6B). This is consistent with the result of Fig. 5B, which also suggested that the delay time used ($\tau = 1$) was inappropriate for this intermediate air flow case. Indeed, a time delay of 1 is unlikely to have any physical significance at all, representing essentially, electronic noise. When delay times in the range suggested by AMI were used ($\tau = 9$, 14, 15 for Fig. 6A, B, and C, respectively), only Fig. 6B changed significantly, becoming more like Fig. 6A. Finally when the air flow is high, the points are dispersed all over the phase space plot (Fig. 6C). This indicates two aspects: the delay time may be too large, or the system is in a very chaotic regime. From Fig. 5C we observed that the delay time was appropriate, and therefore, the second inference that the regime is very chaotic is more believable.

For the pressure time series, the points are close to diagonal for the three air flow rates, though for the moderate air flow two diagonals are observed (Fig. 6E). From Fig. 5B the delay time is appropriate, and therefore, the phase space indicates that the system is in a transitional regime. Some points are dispersed away from the diagonal for the high flow rate, and as in the equivalent acoustic case this is probably because that the system is in a very chaotic regime (Fig. 6F). When delay times in the range suggested by AMI was used ($\tau = 4$, 6, 4 for Fig. 6D, E, and F, respectively), these Figs. 6D, E, and F did not change significantly.

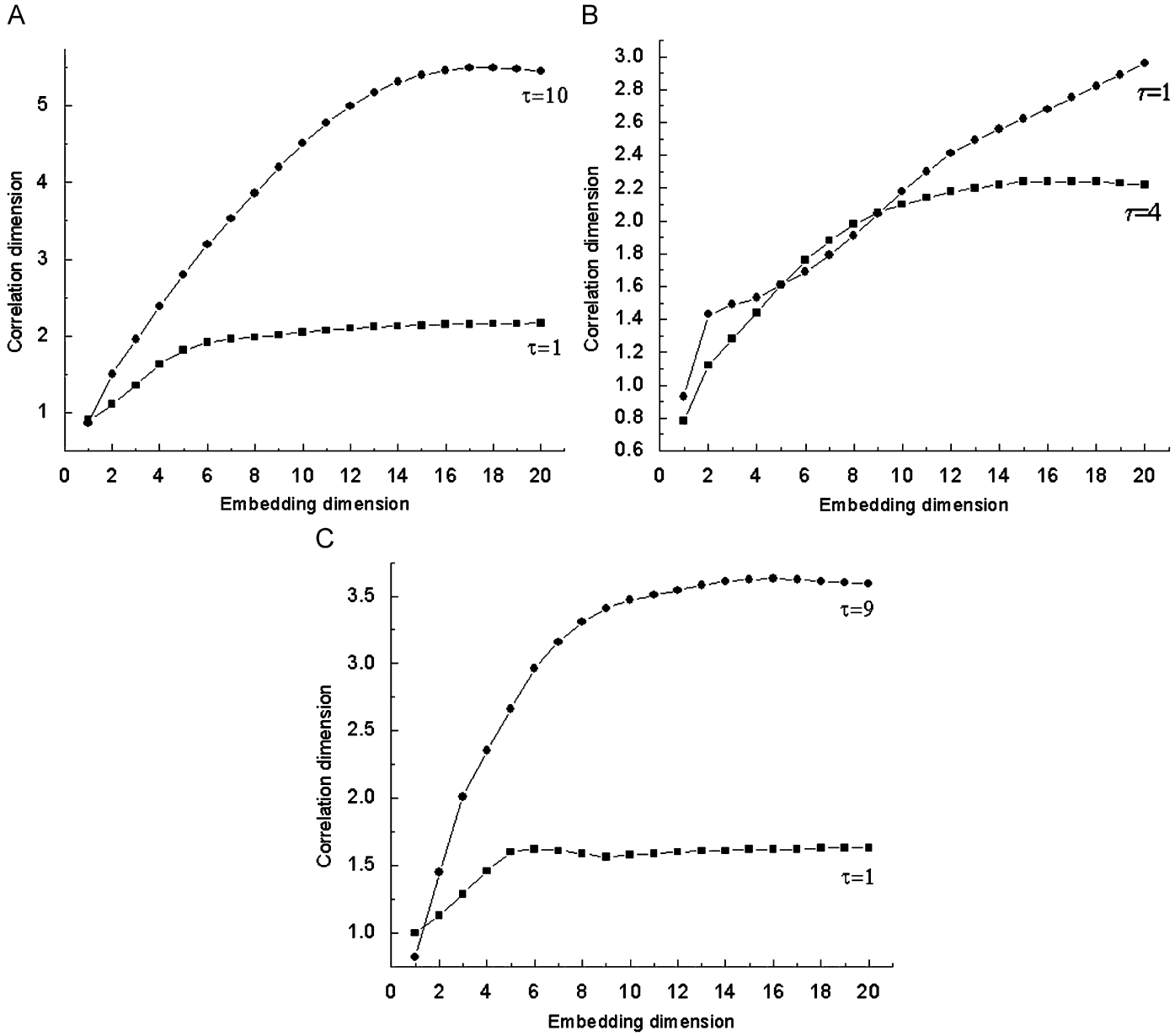

Fig. 5. Correlation dimension (D_2) plots for low (A), moderate (B), and high (C) flow rates for pressure (square) and acoustic (circles) signals.

In order to confirm the regimes identified above, the RPs were computed and are shown in Fig. 7 for the pressure case ($\tau = 1$ for each flow rate) and Fig. 8 for the acoustic case ($\tau = 10$, 4, 9, respectively).

In the pressure case, the structure of the RP for the low air flow rate is formed from slightly deformed diagonal lines (Fig. 7A), while for the moderate flow rate the diagonals exhibit dispersed points. For the high flow rate the dispersed points disappear, but the diagonals now are broken. The foregoing indicates that when the air flow rate is increased, the system changes from a stable to a chaotic state (Fig. 7). However, in the acoustic case, even for the low air flow rate (Fig. 8A) the RP does not shown any clear structure and when the air flow is high (Fig. 8C) the recurrence map exhibits many dispersed points indicating that the system is very chaotic.

The correlation fractal dimension D_2 for both signals as a function of air flow rate Q is shown in Fig. 9.

At first as Q increases, D_2 decreases from 5.5 to 4.3 for the acoustic case, while for the pressure case D_2 rises slightly to 2.2 and falls to 1.9. This delineates Region I. As Q increases further, the D_2 rise slightly and then fall, from 3.8 to 3.4 for the acoustic case, and from 2.5 to 1.8 for the pressure case. This delineates Region II. Finally, in Region III, the D_2 values change from 3.6 to 3.65 (acoustic) and from 2.2 to 1.6 (pressure).

Similar D_2 behavior for the pressure signals was observed in the experimental work of Liu (2003) for a gas–liquid bubble column. In Liu (2003), when the gas flow rate was increased, a sequence of periodic bubbling, primary-advanced chaotic bubbling, and jetting or random bubbling was successively observed. In our study, these flow regimes correspond to Regions I, II, and III.

In Region I, individual bubbles are generated, the pressure–acoustical signals are easily identified and the biphase system is stable. Region II is characterized by changes in the bubbling dynamics, bubble coalescences appear and the biphase system is in a transition regime. In the third region, stability is totally lost; an air jet dominates the bubbling dynamics and the biphase system is random.

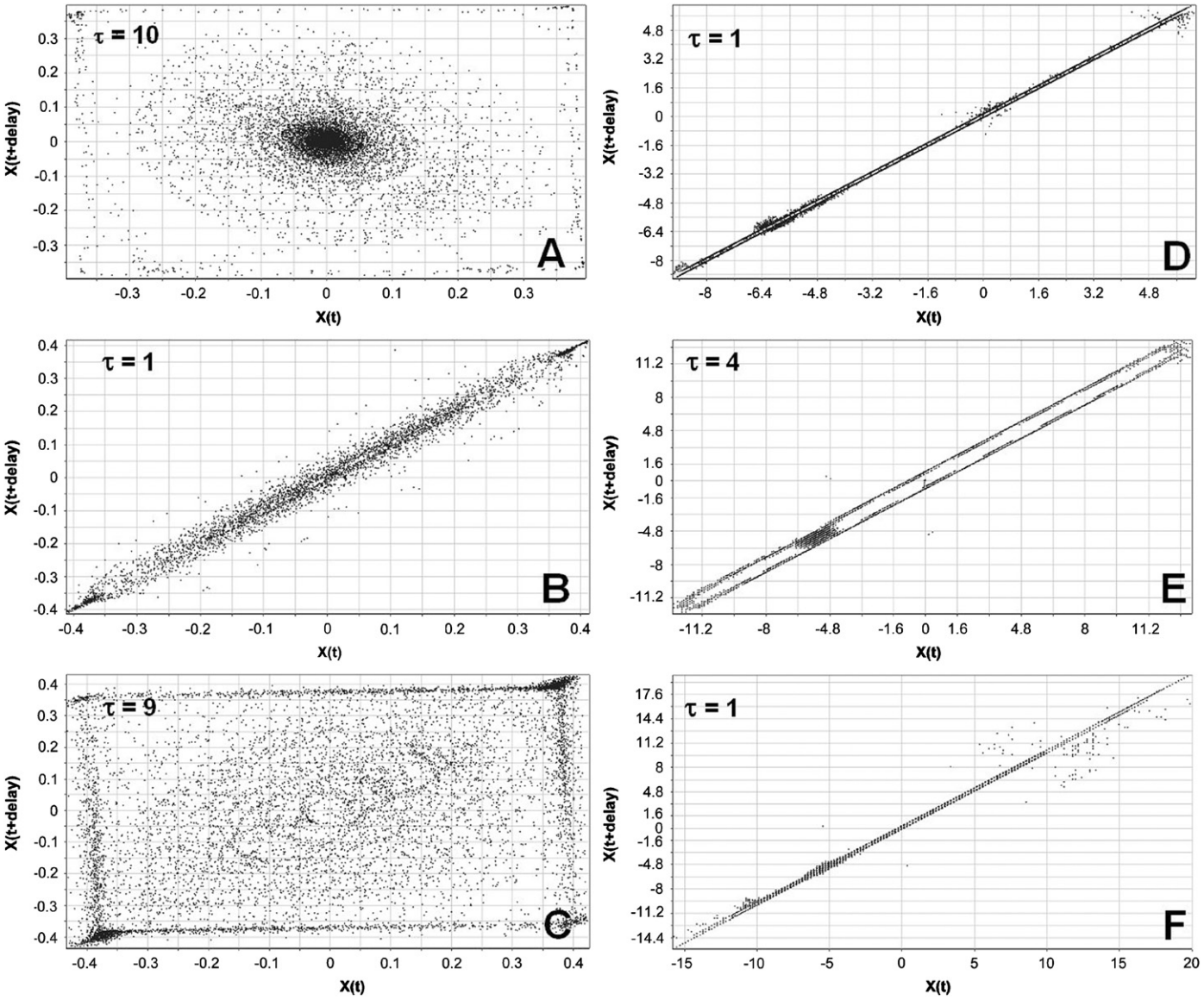

Fig. 6. Phase space for low (A), moderate (B), and high (C) flow rate for the acoustic case, in which $\tau = 10$, 1, 9, respectively, and low (D), moderate (E), and high (F) for the pressure case, in which $\tau = 1$, 4, 1, respectively.

Recently Al-Masry et al. (2007) calculated the standard deviation (σ) of the acoustic and differential pressure signals recorder in air–water system. Al-Masry et al. used a Perspex bubble column with superficial gas velocities of 0.009–0.094 m s^{-1} in a gas distributor with 85 holes of 1 mm diameter equally distributed. They found two transition points at 176 and 264 ml min^{-1} for the acoustic and at 148 and 232 ml min^{-1} for the differential pressure fluctuations; in both cases the standard deviation increased monotonically when the superficial gas velocity was incremented. In our study the σ also show two transition points and a similar behavior (Fig. 10).

Experiments on bubble production in only marginally different experimental systems often show markedly different results owing to differences in tank sizes, injection systems, and the location and type of measurement systems. There are several aspects to consider in interpreting the present results in relation to similar work in the literature. Firstly, in the work of Liu (2003) the pressure transducer probe was placed in the liquid near to the nozzle. Although such a system is subject to noise (liquid movement, wake influence, etc.), in comparing Liu's results with ours (where the pressure transducer is located in capillary base and free of such noise), the behavior is very similar in general. This suggests that the low-pass filter applied by Liu (2003) was suitable. In Al-Masry et al. (2007) the differential pressure meter was placed outside of the column, reading between two points at the column wall. For this reason, the pressure fluctuations were very different to those observed in Fig. 2; therefore, the standard deviation results of Al-Masry et al. (2007) do not show the transition points as clearly as in Fig. 10.

Secondly, when Cieslinski and Mosdorf (2005) applied the chaotic technique to acoustic as well as laser signals, they obtained the maps of chaotic attractors for several volume flow rates (42, 125, and 233 ml min^{-1}) in which all attractors displayed chaotic character. The three regions of Liu (2003) and the present study were not observed. This may be because the hydrophone in Cieslinski and Mosdorf's case was very close (1 cm) to the bubble formation point, for bubble diameters in the order of several millimeters. Hence, the hydrophone could have influenced the bubble formation; unlike the present signals (Fig. 2), their acoustic signals showed very significant variability, indicating they were influenced by both acoustic

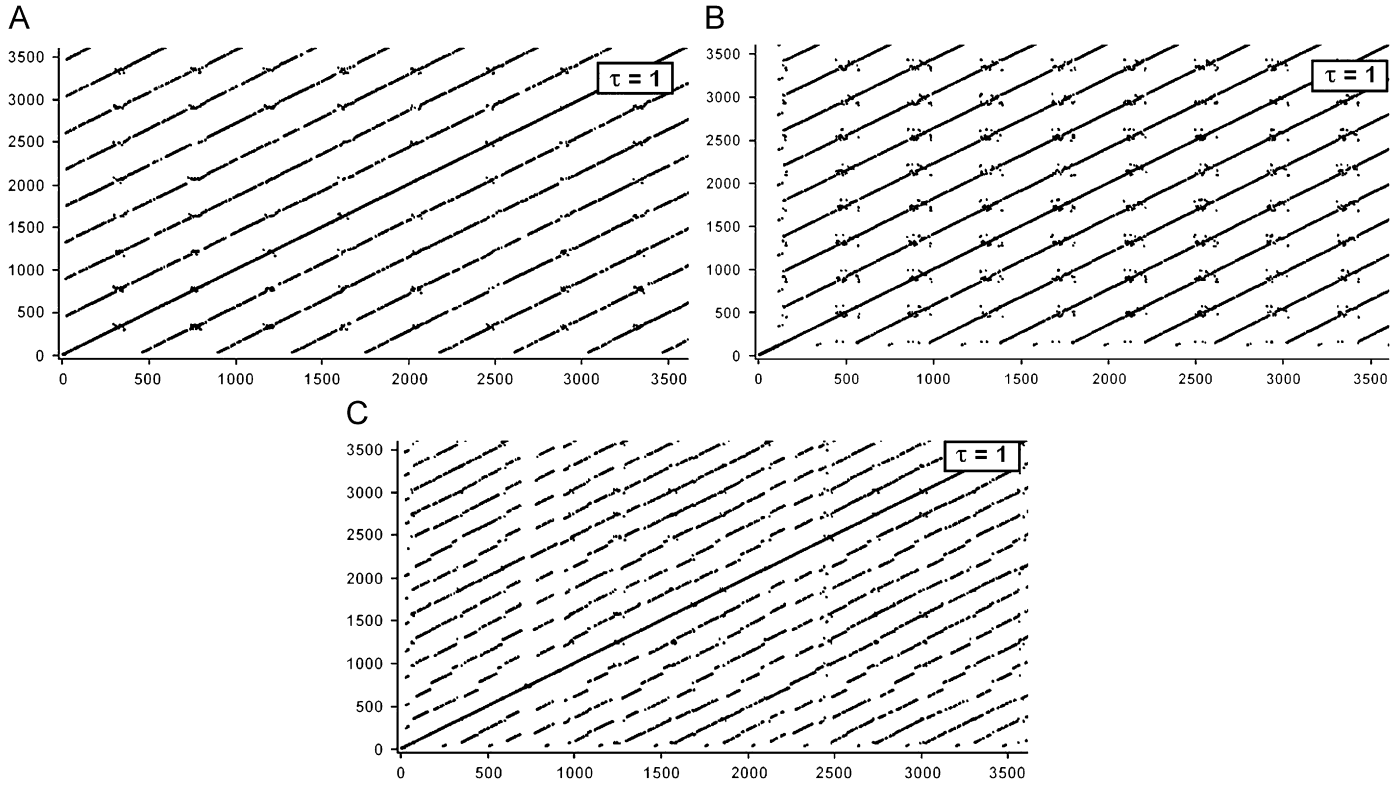

Fig. 7. Recurrence plots for low (A), moderate (B), and high (C) flow rates for pressure signals; $\tau = 1$ for each flow rate.

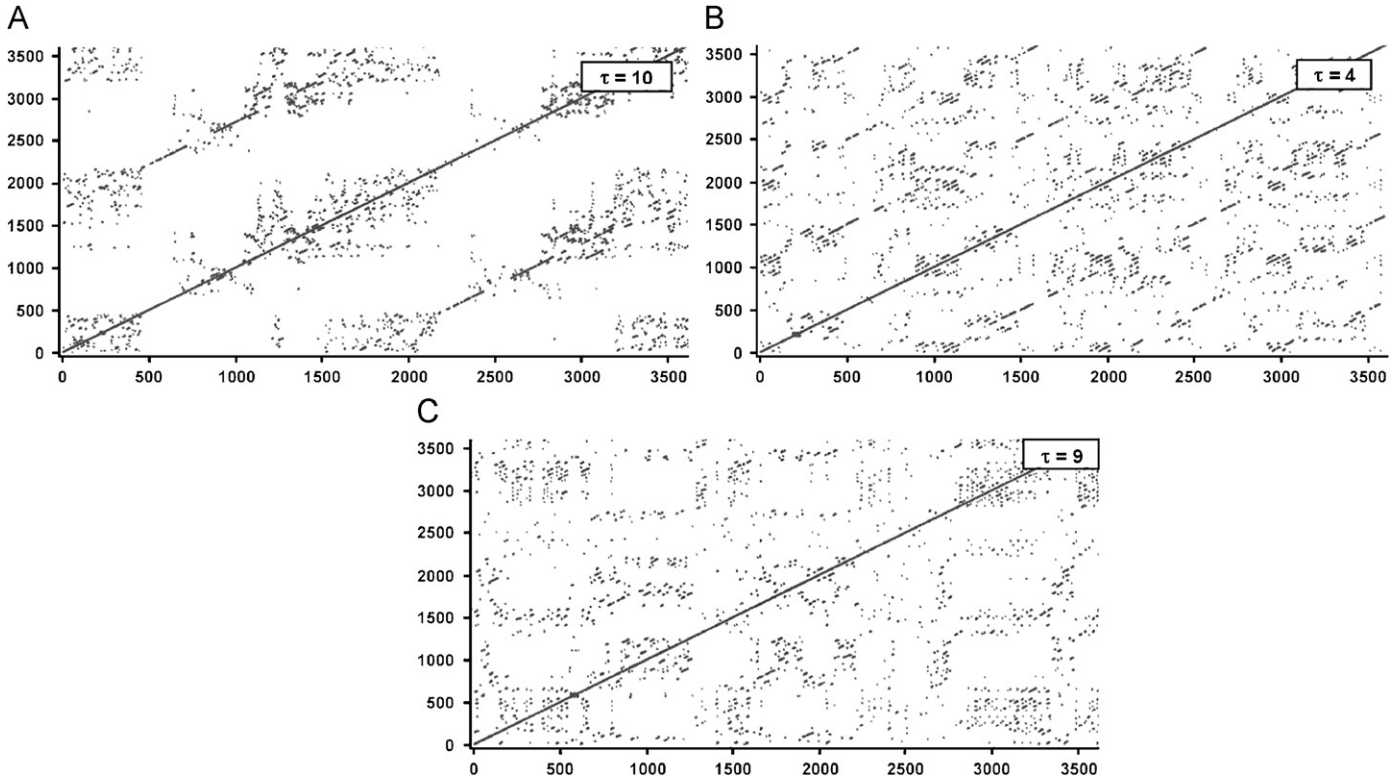

Fig. 8. Recurrence plots for low (A), moderate (B), and high (C) flow rates for acoustic signals; $\tau = 10, 4, 9$, respectively.

and pressure–fluid dynamical phenomena. In addition they did not observe bubble coalescence for volume flow rates less than $233\,\mathrm{ml\,min^{-1}}$; in the present study this air flow rate is located in Region II in bubbles coalescences occur.

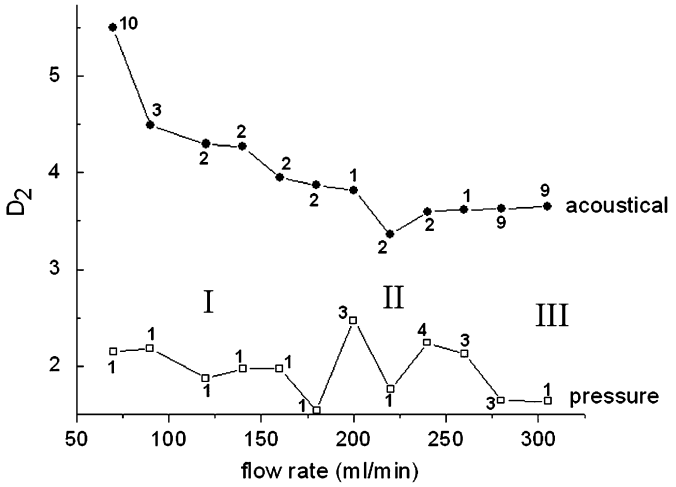

Fig. 9. Correlation dimension for the acoustic and pressure cases; the delay time for each point is noted next to each data point.

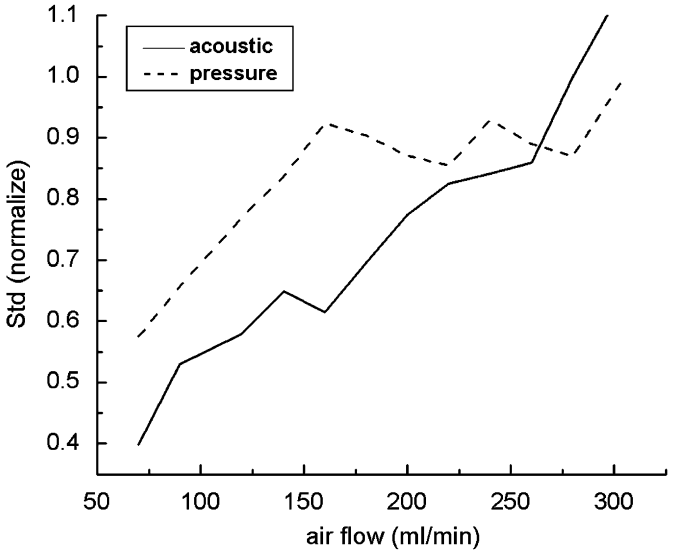

Fig. 10. Standard deviation for acoustic and pressure cases.

Thirdly, the saturation value of embedding dimension was not reached for moderate air flow rates for the acoustic signals. This may be because of bistability (in which two stable periodic regimes exist for the same air flow rate) in Region II. Consequently, the proper estimation of the correlation dimension is difficult. However, to confirm this speculation a future detailed study is necessary.

5. Conclusions

Experiments were performed on both the acoustic and pressure signals produced by bubbles formed from an underwater nozzle. The data were analyzed by a comprehensive set of spectral and nonlinear dynamical systems techniques. The present study of both acoustic and pressure signals showed that the chaos appeared in different regimes and was manifested in different ways in the acoustic and pressure signals. The use of different time delays for the chaotic analysis of acoustic and pressure signals was found necessary and in the case of moderate air flow rates an appropriate time delay could not be found. The acoustic signals offer data primarily on the bubble size while the pressure signals offer data primarily on the bubble production rate. The present results are in good agreement with the work of Liu (2003) for the pressure case. It appears that dynamical systems analyses give different results for acoustic and pressure signals, despite attempts to optimize the analyses, possibly owing to the dramatic (100X) difference in timescales.

The present results suggest that chaos need not be manifested in the bubble size and bubble production rate simultaneously or in exactly the same regime. This is consistent with the well-known observation that changes in air flow rate can affect bubble size and bubble production rate to different extents in different air flow regimes (Clift et al., 1978).

A first conclusion is that caution should be exercised in analyzing either acoustic or pressure signals in isolation, and that simultaneous measurement of both are ideal. However, a second, more promising conclusion is that acoustic and pressure measurements could be used to probe different aspects of a gas sparging system. For example, chaos in the acoustic signal could indicate a broadening of the bubble size distribution, which has relevance for the local gas–liquid mass transfer co-efficient, while chaos in the pressure signal could indicate the overall multiphase flow has become turbulent, which has implications for the overall transport properties of the flow. For this application of acoustic-pressure measurement to be developed, further careful chaotic studies of both acoustic and pressure signals will be necessary. Owing to the very large difference in timescales, careful thought will be required into new ways to process the data.

Notation

d	embedding dimension, dimensionless
D_2	correlation dimension, dimensionless
f_0	frequency, Hz
P_∞	absolute liquid pressure, Nm^{-2}
Q	flow rate, $\mathrm{ml\,min}^{-1}$
r	radius of dimension ball
R_0	equivalent bubble radius, m

Greek letters

γ	specific heats ratio, dimensionless
δ	closeness, %
θ	heaviside step function
ρ	liquid density, $\mathrm{Kg\,m}^{-3}$
τ	time delay, dimensionless

Acknowledgments

The authors gratefully acknowledge Prof. Elizabeth Salinas and Alberto Soria for the equipment support at Universidad Autónoma Metropolitana—Iztapalapa.

References

Abarbanel, H.D.I., 1996. Analysis of Observed Chaotic Data. Springer, New York.
Al-Masry, W., Ali, E., Aqeel, Y., 2005. Determination of bubble characteristics in bubble columns using statisticals análisis of acoustics sound measurements. Chemical Engineering Research and Design 83, 1196–1207.
Al-Masry, W., Ali, E., Al-Kalbani, M., 2007. Prediction of regime transitions in bubble columns using acoustic and differential pressure signals. Chemical Engineering Journal 133, 139–149.
Atay, F.M., Altintas, Y., 1999. Recovering smooth dynamics from time series with the aid of recurrence plots. Physical Review E 59 (6), 6593–6598.
Barghi, S., Prakash, A., Margaritis, A., Bergougnou, M.A., 2004. Flow regime identification in a slurry bubble column from gas holdup and pressure fluctuations analysis. The Canadian Journal of Chemical Engineering 82, 865–870.
Briens, A.L., Ellis, N., 2005. Hydrodinamics of three-phase fluidized bed systems examined by statistical, fractal, chaos and wavelet analysis methods. Chemical Engineering Science 60, 6094–6106.
Chilekar, V.P., Warnier, M.J.F., van der Schaaf, J., Kuster, B.F.M., Schouten, J.C., van Ommen, J.R., 2005. Bubble size estimation in slurry bubble columns from pressure fluctuations. AIChE Journal 51, 1924–1937.

Cieslinski, J.T., Mosdorf, R., 2005. Gas bubble dynamics-experiment and fractal analysis. International Journal of Heat and Mass Transfer 48 (9), 1808–1818.
Clift, R., Grace, J.R., Weber, M.E., 1978. Bubbles, Drops and Particles. Academic Press, London.
Ding, M., Greogi, C., Ott, E., Sauer, T., Yorke, J.A., 1993. Estimating correlation dimension from a chaotic time series: when does plateau onset occur? Physica D 69, 404–424.
Eckmann, J.P., Kamphorst, S.O., Ruelle, D., 1987. Recurrence plots of dynamical systems. Europhysics Letters 4 (9), 973–977.
Fan, J., Yao, Q., 2005. Nonlinear Time Series: Nonparametric and Parametric Methods. Springer, New York.
Fan, L.S., Satija, S., Wisecarver, K., 1986. Pressure fluctuation measurements and flow regime transitions in gas–liquid–solid fluidized beds. AIChE Journal 32, 338–340.
Fan, L.T., Ho, T.C., Hiraoka, S., Walawender, W.P., 1981. Pressure fluctuations in a fluidized bed. AIChE Journal 27, 388–396.
Filderis, V., Whitmore, R.L., 1961. Experimental determination of the wall effect for spheres falling axially in cylindrical vessels. British Journal of Applied Physics 12, 490.
George, D.L., Torczynski, J.R., Shollenberger, K.A., Ohern, T.J., Ceccio, S.L., 2000. Validation of electrical-impedance tomography for measurements of material distribution in two-phase flow. International Journal of Multiphase Flow 26, 549–581.
Graham, A., Woolf, D.K., Hall, A.J., 2004. Aeration due to breaking waves. Part I: bubble populations. Journal of Physical Oceanography 34, 989–1007.
Hubersa, J.L., Striegelb, A.C., Heindela, T.J., Grayb, J.N., Jensenb, T.C., 2005. X-ray computed tomography in large bubble columns. Chemical Engineering Science 60, 6124–6133.
Hulmea, I., Kantzasa, A., 2004. Determination of bubble diameter and axial velocity for a polyethylene fluidized bed using X-ray fluoroscopy. Powder Technology 147, 20–33.
Johnson, B.D., 1986. Bubble populations: background and breaking waves. In: Monahan, E.C., MacNiocail, G. (Eds.), Oceanic Whitecaps and their Role in Air–Sea Gas Exchange Processes. D. Reidel Publishing Company, Hingham, MA, USA, pp. 69–76.
Johnsson, F., Zijerveld, R.C., Schouten, J.C., van den Bleek, C.M., Leckner, B., 2000. Characterization of fluidization regimes by time-series analysis of pressure fluctuations. International Journal of Multiphase Flow 26, 663–715.
Kinsler, L.E., Frey, A.R., 1962. Fundamentals of Acoustics. Wiley, New York.
Klein, J., Rosenberg, M., Markos, J., Dolgos, O., Kroslak, M., Kristofikova, L., 2002. Biogeneration of glucose to gluconic acid by *Aspergillus niger*—study of mass transfer in an airlift bioreactor. Biochemical Engineering Journal 10, 197–205.
Koynov, A., Khinast, J.G., 2004. Effects of hydrodynamics and lagrangian transport on chemically reacting bubble flows. Chemical Engineering Science 59, 3907–3924.
Krishna, R., de Swart, J.W.A., Ellenberger, J., Martina, G.B., Maretto, C., 1997. Gas holdup in slurry bubble columns: effect of column diameter and slurry concentrations. AIChE Journal 43, 311–316.
Kung-Sik, C., Howell, T., 2001. Chaos: A Statistical Perspective. Springer, New York.
Lee, H.C., Oh, B.D., Bae, S.W., Kim, M.H., 2003. Single bubble growth in saturated pool boiling on a constant wall temperature surface. International Journal of Multiphase Flow 29, 1857–1874.
Leifer, I., Patro, R.K., 2002. The bubble mechanism for transport of methane from the shallow sea bed to the surface: a review and sensitivity study. Continental Shelf Research 22, 2409–2428.
Lin, T.J., Juang, R.C., Chen, Y.C., Chen, C.C., 2001. Predictions of flow transitions in a bubble column by chaotic time series analysis of pressure fluctuations signals. Chemical Engineering Science 56, 1057–1065.
Liu, M., 2003. Nonlinear bubbling hydrodynamics in a gas–liquid bubble column with a single nozzle. International Journal of chemical reactor engineering 1 article A32.
Loewen, M., Melville, W., 1991. A model of the sound generated by breaking waves. Journal of Acoustical Society of America 90, 2075–2080.
Manasseh, R., La Fontaine, R.F., Davy, J., Sheperd, I., Zhu, Y.G., 2001. Passive acoustic bubble sizing in sparged systems. Experiments in Fluids 30, 672–682.
Manasseh, R., Nikolovska, A., Ooi, A., Yoshida, S., 2004. Anisotropy in the sound field generated by a bubble chain. Journal of Sound and Vibration 278, 807–823.
Manasseh, R., Riboux, G., Risso, F., 2008. Sound generation on bubble coalescence following detachment. International Journal of Multiphase Flows, in press, doi:10.1016/j.ijmultiphaseflow.2008.03.005.
Manley, D., 1960. Change of size of air bubbles in water containing a small dissolved air content. British Journal of Applied Physics 11, 38–42.
Mindlin, G.B., Solari, H.G., Natiello, M.A., Gilmore, R., Hou, X.-J., 1991. Topological analysis of chaotic time series data from the Belousov–Zhabotinskii reaction. Nonlinear Science 1, 147–173.
Minnaert, M., 1933. On musical air-bubbles and sounds of running water. Philosophical Magazine 16, 235–248.
Mosdorf, R., Shoji, M., 2003. Chaos in bubbling-nonlinear analysis and modeling. Chemical Engineering Science 58, 3837–3846.
Nerenberg, M.A.H., Essex, C., 1990. Correlation dimension and systematic geometric effects. Physical Review A 42 (12), 7065–7074.
Nguyen, K., Daw, C.S., Chakka, P., Cheng, M., Bruns, D.D., Finney, C.E.A., Kennel, M.B., 1996. Spatio-temporal dynamics in a train of rising bubbles. Chemical Engineering Journal 64, 191–197.
Nikolovska, A., 2005. Passive acoustic transmission and sound channelling along bubbly chains. Ph.D. thesis, Department of Mechanical and Manufacturing Engineering, University of Melboune, Australia.
Oliveira, M.S.N., Ni, X.W., 2004. Characterization of a gas–liquid obc: bubble size and gas holdup. AIChE Journal 50, 3019–3033.
Prakash, A., Margaritis, A., Li, H., Bergougnou, M.A., 2001. Hydrodynamics and local heat transfer measurements in a bubble column with suspension of yeast. Biochemical Engineering Journal 9, 155–163.
Raffensberger, J.A., Glasser, B.J., Khinast, J.G., 2005. Analysis of heterogeneously catalyzed reactions close to bubbles. AIChE Journal 51 (5), 1482–1496.
Ruzicka, M.D., Zahradnik, J., Thomas, N.H., 2000. Homogeneous-heterogeneous regime transition in bubble columns. Chemical Engineering Science 55, 421–429.
Satija, S., Fan, L.S., 1985. Characteristics of slugging regime and transition to turbulent regime for fluidized beds of large coarse particles. AIChE Journal 31, 1554–1562.
Sato, M., Kuroda, M., Sakai, T., 1979. Effect of electrostatics on bubble formation. Kagaku Kogaku Ronbunshu 5, 380–384.
Shah, Y.T., Deckwer, W.D., 1985. In: Bisio, Kabel, R.L. (Eds.), Fluid–Solid Reactors in Scale-up of Chemical Processes. Wiley, New York.
Shin, W.T., Yiacoumi, S., Tsouris, C., 1997. Experiments on electrostatics dispersion of air in water. Industrial and Engineering Chemistry Research 36, 3647–3655.
Sun, J.G., Chen, M.M., Chao, B.T., 1994. Modeling of solids global fluctuations in bubbling fluidized beds by standing surface waves. International Journal of Multiphase Flow 20, 315–338.
Takens, F., 1981. Detecting strange attractors in turbulence. In: Rand, D.A., Young, L.S. (Eds.), Dynamical System and Turbulence. Springer, Berlin.
Teresaka, K., Prakoso, T., Tsuge, H., 2000. Two-phase bubble formation with condensation at a nozzle submerged in immiscible liquid. Chemical Engineering (Japan) 33, 113–119.
Tufaile, A., Sartorelli, J.C., 2000. Chaotic behavior in bubble formation dynamics. Physica A 275, 336–346.
Tufaile, A., Pinto, R.D., Goncalves, W.M., Sartorelli, J.C., 1999. Simulations in a dripping faucet experiment. Physics Letters A 255, 58–64.
van der Schaaf, J., Johnsson, F., Schouten, J., van den Bleek, C.M., 1999. Fourier analysis of nonlinear pressure fluctuations in gas–solid flow in CFB risers—observing solids structures and gas/particle turbulence. Chemical Engineering Science 54, 5541–5546.
van der Schaaf, J., Schouten, J.C., Johnsson, F., van den Bleek, C.M., 2002. Non-intrusive determination of bubble and slug length scales in fluid beds by decomposition of the power spectral density of pressure time series. International Journal of Multiphase Flow 28, 865–880.
Vazquez, A., Sanchez, R.M., Salinas-Rodríguez, E., Soria, A., Manaseeh, R., 2005. A look at three measurement techniques for bubbles size determination. Experimental Thermal and Fluid Sciences 30, 49–57.
Vergniolle, S., Brandeis, G., 1996. Strombolian explosions 1. A large bubble breaking at the surface of a lava column as a source of sound. Journal of Geophysical Research 101 (B9), 20433–20447.
Walter, J.F., Blanch, H.W., 1986. Bubble break-up in gas–liquid bioreactors: break-up in turbulent flows. Chemical Engineering Journal 32, B7.
Wang, M., Yin, W., Holliday, N., 2002. A highly adaptive electrical impedance sensing system for flow measurement. Measurement Science and Technology 13, 1884–1889.
Xie, S., Tan, R.B.H., 2003. Bubble formation at multiple orifices—bubbling synchronicity and frequency. Chemical Engineering Science 58, 4639–4647.
Zenit, R., Koch, D.L., Sangani, A.S., 2003. Impedance probe to measure local gas volume fraction and bubble velocity in a bubbly liquid. Review of Scientific Instruments 74, 2817–2827.
Zhang, L., Shoji, M., 2001. A periodic bubble formation from a submerged orifice. Chemical Engineering Science 56, 5371–5381.
Zukowski, W., 2001. An acoustic method of studying sequential explosions during gas combustion in bubbling fluidized beds. Combustion and Flame 125, 1075–1082.